Exploring Novel Methods of Interferometric Detection of Ultrasmall Phase Shifts

Jaesuk Hwang[a,b], Martin M. Fejer[a], and W.E. Moerner[b]
[a]Department of Applied Physics, Stanford University
[b]Department of Chemistry, Stanford University

ABSTRACT

We propose a new method to detect ultrasmall nonreciprocal phase shifts in solids based on the Sagnac interferometer combined with internal optical modulation of the absorption. The Sagnac interferometer with heterodyne balanced detection is expected to enable shot-noise-limited detection of phase shift as a result of its insensitivity to frequency and amplitude fluctuations of the laser. The low-concentration molecular sample is internally modulated by optical saturation with a pulsed laser. This internal modulation makes the molecular absorption time-dependent, and also removes the possibility of amplitude modulation feedthrough. We describe the design of this experiment and present preliminary characterizations of the noise performance.

Keywords: ultrasensitive detection, molecular absorption, Sagnac interferometer, modulation spectroscopy

1. INTRODUCTION

Current ultrasensitive detection experiments in fields ranging from materials science to biophysics often make use of labeling with highly fluorescent molecules such as laser dyes or autofluorescent proteins. In spite of some advantages, labeling with extrinsic fluorophores can produce unwanted perturbations to the system to a degree that may be hard to quantify. Moreover, sensitive detection of fluorescence in general presents a host of experimental issues, most notably the need to rigorously exclude from the probed volume all sources of unwanted fluorescence or Raman scattering and count single photons.

An alternative detection method that we consider here is absorption spectroscopy, in which the absorption events are not detected by recording fluorescence. In this case, any spurious fluorescence from the sample or substrate are not important, and all the photons in the entire laser beam probing the sample can be used to sense the signal of interest. Frequency-modulated absorption spectroscopy was the first method to enable detection and spectroscopy of single molecules in condensed matter in 1989 [1]; however, these experiments utilized liquid helium temperatures to produce narrow absorption profiles and absorption cross sections near the maximum possible values on the order of the optical wavelength squared. Here we concentrate on room temperature detection, which represents a considerable challenge because the absorption cross sections are ~ 10^5 times smaller than in the earlier low temperature experiments.

Absorption of a photon by a molecule necessarily results in a phase shift of the probing beam. Instead of directly measuring the absorption, we choose to detect this phase shift interferometrically. Among many forms of interferometers, the Sagnac interferometer, which is routinely used for optical gyroscopes, was recently proposed for the particularly challenging application of gravitational wave detection [2,3]. Among several appealing features, the Sagnac interferometer is largely insensitive to amplitude and phase noise of the probe beam and only sensitive to nonreciprocity in the loop, i. e. the phase difference between two counter-propagating beams. This nonreciprocal phase difference is easy to generate in the case of rotation of the loop or in the case of magneto-optic media. For a more general sample with a nonmagnetic molecular absorption, the refractive index (or optical absorption) of the sample can be modulated in a time-dependent manner, and the sample placed asymmetrically in the Sagnac loop, in order that the clockwise and counter-clockwise beams encounter different phase shifts. This modulation of the refractive index could be accomplished by physically dithering the sample, e.g. by ultrasonic time-varying fields; however, in this work we utilize a second pumping laser at a different wavelength to produce time-dependent optical saturation of the sample.

In the second section, we estimate the phase shift resulting from absorption, using a single-molecule as the ultimate unit of absorption. The third section describes the working principle of the Sagnac

Manipulation and Analysis of Biomolecules, Cells, and Tissues,
Dan V. Nicolau, Jörg Enderlein, Robert C. Leif, Daniel L. Farkas, Editors,
Proceedings of SPIE Vol. 4962 (2003) © 2003 SPIE · 1605-7422/03/$15.00

interferometer we use. The fourth section explains how we modulate the sample to obtain a time-dependent signal out of the interferometer. In the fifth section, the detection scheme is presented and shot-noise-limited signal-to-noise ratio is calculated. We present measurements on the noise spectral density of the apparatus that illustrates the feasibility of this scheme in the sixth section.

2. ESTIMATE OF PHASE SHIFT FROM ABSORPTION

The optical absorption and phase shift are intimately connected by a fundamental law of electrodynamics, namely the well-known Kramers-Kronig relation [4]. The formulation of this relation most appropriate in the present context relates the refractive index change per density of molecules, κ, to the absorption cross section σ and the incident probe beam frequency ω:

$$\kappa(\omega) = \frac{c}{\pi} \mathrm{P} \int_0^\infty \frac{\sigma(\omega')}{\omega'^2 - \omega^2} d\omega'$$

where c is the speed of light, and P represents the Cauchy principal value of the integral. Therefore the phase shift from one molecule for a probe beam focused to a spot of area A would be

$$\delta(\omega) = \frac{2\pi}{\lambda A} \kappa(\omega)$$

with σ, λ, and A kept in the same units. Using the formulas above, a useful estimate of the phase shift from one molecule can be determined from a measurement of the absorption spectrum of a bulk sample of known concentration.

Figure 1 shows the absorption cross section (per molecule) obtained from the measured absorption spectrum of Cy5 dye molecules taken in pH 7 buffer at concentration 10^{-5} M. The single-molecule phase shift was calculated from this spectrum assuming 1 μm^2 spotsize for the probing beam. This calculation tells us that if the system is sensitive enough to detect ~ 10^{-9} rad phase change, there is a chance that we can detect a single Cy5 molecule at room temperature. (Strictly speaking, for a single molecule, it is the probability of absorption or dispersion that controls the interaction between the light field and the molecule. In actual experiments, a time-average of many photons interacting with the molecule is measured, and if this average samples ergodically, the final result effectively mimics the usual ensemble-averaged behavior of a bulk sample.)

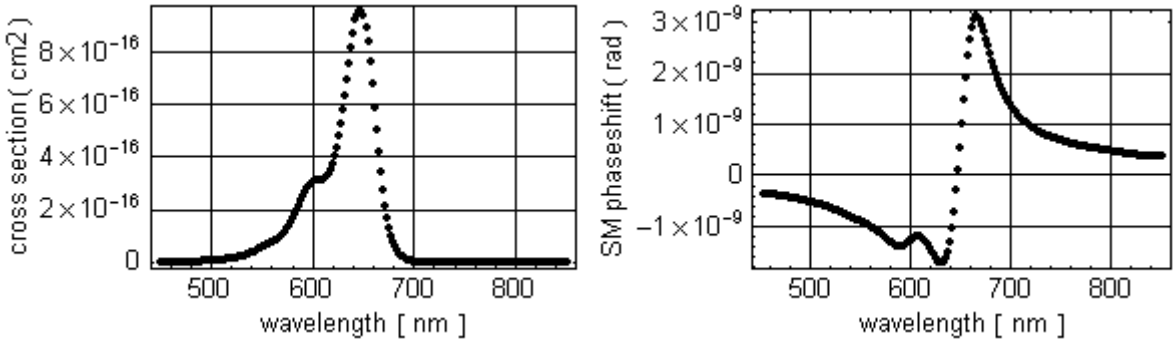

Figure 1: The left panel shows the absorption cross section per molecule calculated from the bulk absorption spectrum of Cy5 molecules in aqueous solution. The right panel is the corresponding phase shift per molecule.

3. POLARIZATION SAGNAC INTERFEROMETER

In general, interferometers are designed for sensitive detection of phase shifts, where a laser beam is split into two, one beam experiences the phase change, and the two beams are subsequently recombined to convert the phase change into an amplitude change. A modulated phase difference between two beams results in intensity modulation after recombination. In the case of the Sagnac interferometer [5], since the two counter-propagating beams follow exactly the same path inside the interferometer loop, the resultant intensity signal after recombination is largely insensitive to the phase noise of the probe beam. Moreover,

due to its inherent symmetry, the Sagnac interferometer requires no active control. Other geometries, such as the Michelson interferometer, require active feedback to maintain a constant path difference between the two arms, and fluctuations in this active feedback control can be a major source of noise. Hence the common-path configuration of the Sagnac interferometer enables us to exclude several possible noise sources that can prevent attainment of shot-noise-limited detection.

In this work, we adopt the polarization Sagnac interferometer [2,3] that was proposed earlier for gravitational wave detection. As shown in Figure 2, the interferometer is composed of two polarizing beam splitters (PBS) and two half wave plates (HWP). Propagation of the probe beam is represented in the diagram by the increment of the numbers. Starting out with $\hat{x}$ polarization, the probe beam passes through the first PBS with only nominal loss due to the orientation of the PBS. Passing through the first HWP (oriented to rotate polarization by 45°), the probe beam is incident on PBS at the entrance to the interferometer loop linearly polarized with a 45° angle from the plane. The probe beam is split in half with the $\hat{x}$-polarized component traveling counterclockwise (CCW) and the $\hat{y}$-polarized component traveling clockwise (CW). The HWP in the interferometer loop is oriented to rotate the plane of polarization by 90°, and thus switches the polarization of the propagating beams between $\hat{x}$ and $\hat{y}$ directions. This ensures that there is only one polarization at a given point around the loop. If the CW beam sees a different amount of phase advance compared to the CCW beam during one round trip, the originally linearly polarized probe beam comes out of the same port of the loop elliptically polarized.

It is useful at this point to connect to the standard terminology of Sagnac interferometers and comment about the "symmetric" and "asymmetric" ports shown in the Figure. For the symmetric port, the

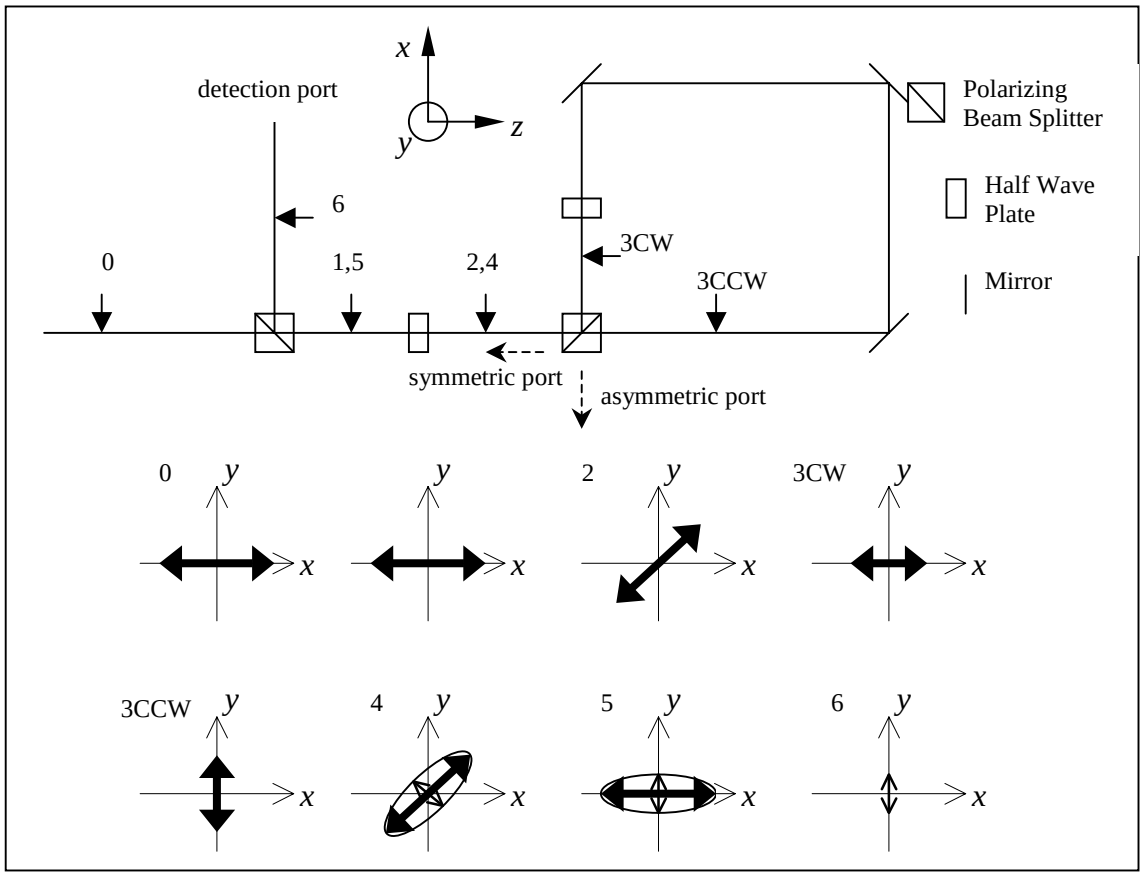

Figure 2: Optical configuration of the polarization Sagnac interferometer. The progression of the probe beam is presented with increasing numbers. The polarization at each point is also shown.

two counter-propagating beams experience one reflection and one transmission each with the same polarization at the beamsplitter. Therefore, even with unequal reflection and transmission coefficients of the PBS, perfect balancing of CW and CCW beams is achieved after recombination. Moreover, the polarization scheme chosen causes the light coming out of the loop to appear completely in the symmetric

port (in the absence of static birefringence in the loop). More importantly, the electric field amplitude of the "dark port", which we define here as the minor axis of the outgoing elliptical beam, is the vector difference between the CW and CCW beams (see below). (Similarly, the major axis is defined as the "bright port" in the same sense.) Hence in the small signal limit, the dark port carries the information about the phase difference between two beams. The outgoing probe beam travels back through the first HWP, and upon encountering the first PBS, mostly the minor axis of the ellipse and only a slight fraction of major axis are reflected to the detection port.

Let us recapitulate the major features of the polarization Sagnac interferometer. First of all, the common path nature of the Sagnac interferometer makes it possible that the zero-background character of the dark port is maintained without any active control and makes the whole system insensitive to the phase noise of the probe laser and any reciprocal nonidealities such as static misalignment (as long as the input and output beams pass through the same single-mode filter). Second, there is only one polarization at a given point along the interferometer loop. This opens up the possibility of polarization sensitive measurement of molecular absorption. Third, a nonreciprocal phase difference between the two counter-propagating beams results in intensity modulation at the dark port. This means the detection port receives negligible optical power in the case of no signal, and the signal has a relatively small DC level compared to the major axis of the outgoing probe beam and the optical power in the loop. This is an improvement over other absorption measurement schemes such as FM spectroscopy in terms of the amount of optical power the photodiode has to tolerate in order to achieve same level of sensitivity. Fourth, the use of the symmetric port allows the darkness of the dark port to be insensitive to the precise specification of the PBS.

On the other hand, the common path nature of the Sagnac interferometer imposes strong constraints on the optical properties of the sample. Since the same sample is seen by both of the counter-propagating beams, the two phase shifts from the sample are cancelled at the dark port. For this reason, the sample must be placed asymmetrically inside the interferometer loop and the refractive index of the sample should be modulated on a time scale comparable to the transit time in the loop in order to create a phase difference between two beams at different times.

Representing the input probe beam as

$$E = E_{in}\mathrm{Cos}\,\omega t$$

the two counter-propagating beams after traveling around the interferometer loop are given by

$$E_{CCW} = E_0\mathrm{Cos}\,\omega t$$
$$E_{CW} = E_0\mathrm{Cos}(\omega t + \Delta\phi)$$
$$\sqrt{\eta_t}\,E_{in} = 2E_0, \text{ with } \Delta\phi = \phi_0 + \delta\phi$$

where η_t is the power transmission factor which takes into account non-equal transmission and reflection coefficients of the PBS, the finite transmission of the HWP, the finite reflection coefficient of the mirrors, and any losses at the spatial filter that will soon be introduced. $\delta\phi(t)$ represents the time-dependent phase shift of the probe beam due to the molecular sample, and ϕ_0 represents the static phase shift due to imperfect alignment and static birefringence of the optics.

Figure 3 depicts the elliptically polarized probe beam at position 5 in the case of a nonzero phase difference between the two counter-propagating beams in the loop. According to the optical configuration of the system, in the ideal case, only the dark port is channeled into the detection port. The intensity response of the dark port is illustrated in the Figure 4. One can see there is negligible optical power reaching the detection port in case of no signal. For nonzero differential phase

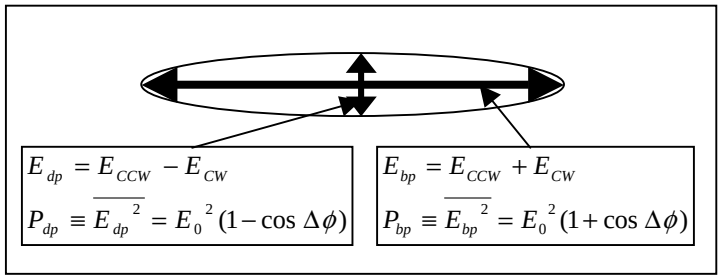

Figure 3: Elliptically polarized probe beam at point 5 in Figure 2. The probe beam exits the interferometer elliptically polarized only when there is phase difference between the CW and CCW beams. The minor axis of this ellipse is defined as the "dark port" and the power in the dark port depends upon the phase difference.

shift, the dark port power P_{dp} is proportional to the square of the phase difference in the small signal limit, i.e.,

$$P_{dp} = P_0(1-\cos\Delta\phi) \cong P_0\Delta\phi^2/2$$

and this quadratic response underscores the necessity of linearizing the signal to increase sensitivity (described below). The contrast ratio, which is often used to appraise the performance of an interferometer, is defined for this specific configuration

$$C \equiv \frac{P_{bp}-P_{dp}}{P_{bp}+P_{dp}} = \cos\Delta\phi \ \cong \cos\phi_0$$

C=1 represents perfect fringe visibility, but in the more general case the contrast ratio is given by the cosine of nonideal static phase difference. In a Sagnac without a single-mode filter, the contrast would be further reduced as described earlier [6].

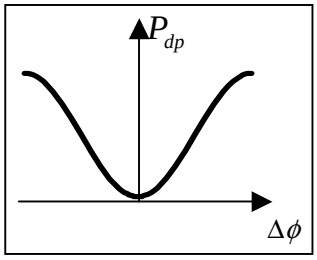

Figure 4: Intensity response of the dark port. The response is proportional to the square of the phase difference in the case that the phase difference is small.

4. SAMPLE MODULATION

So far, we have assumed that the phase difference between the CW and CCW beams $\delta\phi(t)$ is in some way generated by the molecular sample that is placed asymmetrically in the loop. In order to create $\delta\phi(t)$, the CW and CCW beams must be made different, which we choose to accomplish by modulating the refractive index of the sample in a time-dependent manner. If the modulation is periodic, the detection can be performed at a high rf frequency (away from low frequency noise sources), and the detection bandwidth can be reduced to improve sensitivity. In addition, the modulation period should match the effective loop travel time of the probe beam in order to maximize the response. To meet all of these requirements, we choose to exploit the optical saturation behavior of the molecular absorption itself.

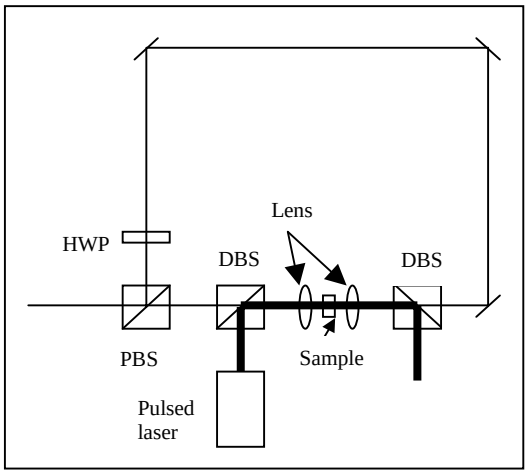

Figure 5: The sample is placed in an asymmetrical position in the loop, and two lenses focus the beam into the sample. The pulsed laser enters the interferometer and saturates the sample with each pulse.

As shown in Figure 5, the sample is placed asymmetrically in the interferometer loop and on a scanning stage in order to ultimately achieve microscopic scanning. Two lenses are used to focus the probe beam into the sample. With the help of a dichroic beam splitter, mode-locked pulsed laser light (at a different wavelength than the probe wavelength) is sent into the interferometer path. Travelling through the same pair of lenses that were used to focus the probe beam, each pump pulse can be chosen to

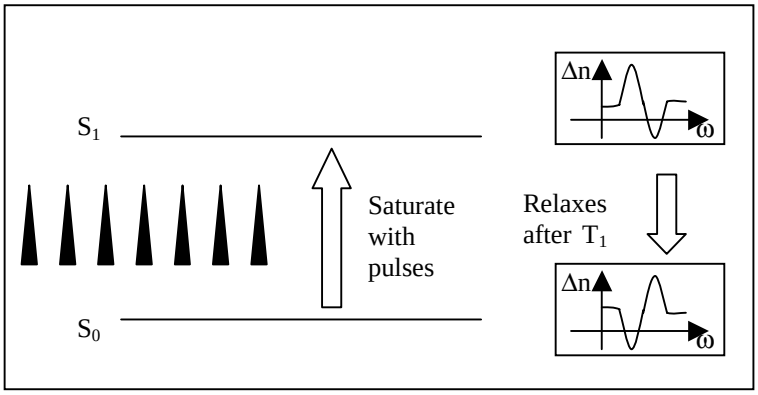

Figure 6: When each pulse places the molecule in the excited state, the dispersion profile changes, and then relaxes after several excited state lifetimes T_1. The wavelength required for excitation can be quite different from the wavelength of maximum phase shift.

saturate the sample; then the pump pulse exits the interferometer loop at another dichroic beam splitter. As Figure 6 illustrates, once a molecule in the sample is excited, the dispersive phase shift spectrum due to the molecule is inverted, recovering its original profile after a time equal to several excited state lifetimes T_1. While the molecule is in the excited state, the probe beam experiences a change in phase shift (at the probe beam wavelength). Figure 7 illustrates this behavior in more detail in the time domain. When the pump pulse is incident on the sample, the refractive index undergoes a change and then recovers. Unless the molecule goes into a long-lived triplet state, this pattern is repeated again for each pump pulse. The CW and CCW beams see the exactly the same change in phase shift due to the sample, but at a different time. The time delay derives from the asymmetric placement of the sample and is given by the effective loop

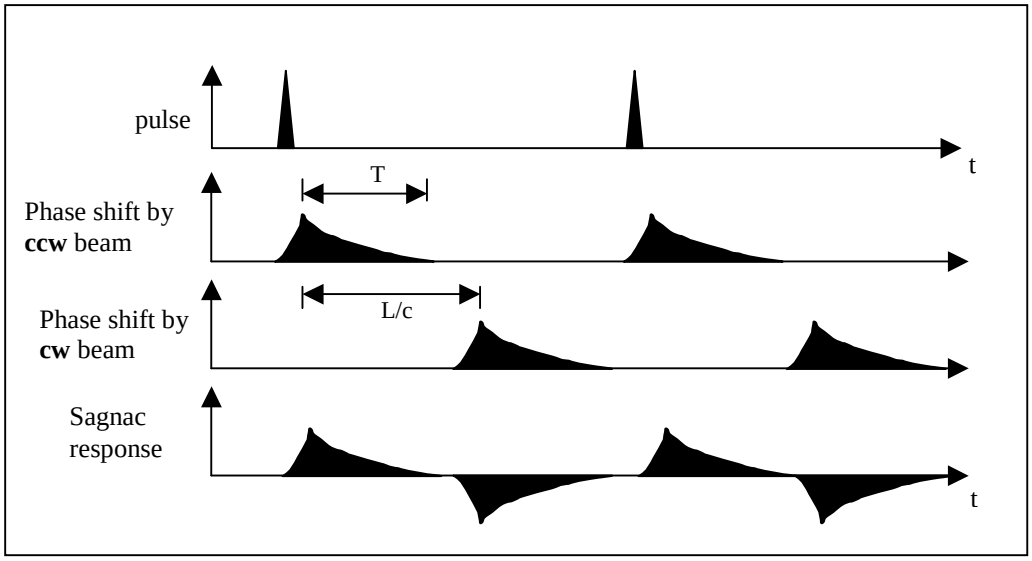

Figure 7: Successive pulses saturate the sample repeatedly and this creates a time dependent index change. CW and CCW beams see the same index changes but at a different time. The time delay is determined by the effective loop length. The final response in the dark port is at the same frequency as the repetition rate of the pulses.

length, which is defined as two times the distance from the sample to the symmetry point at the midpoint of the loop. At the dark port where the vector difference of the CW and CCW electric fields is taken, the response is at the same frequency as the pulse repetition rate. Therefore the signal can be demodulated at the pulse repetition frequency.

By adopting this internal modulation scheme, in which only the sample is subject to time-dependent modulation and the probe laser is not modulated but continuous wave, the possibility of AM feedthrough is removed. (In a similar fashion, internal Stark modulation or strain modulation was used to remove the effects of residual amplitude modulation (RAM) due to imperfections in the electro optic modulator in the earlier low-temperature single-molecule experiments with FM spectroscopy [1].) When AM feedthrough is suppressed, the signal can be averaged as long as desired without losing the signal in the spurious AM.

5. DETECTION SCHEME & SNR

As mentioned earlier and illustrated in Figure 4, the dark port intensity presented to the detection port is proportional to the square of the phase difference between two beams. Since the phase shift we are trying to measure is very small, this makes the signal hard to detect. If we move to the linear region of the response function as indicated in Figure 8, not only will we have more intensity signal for the same phase shift, but also the response is at the same frequency as the phase difference signal, not twice the modulation frequency. Shifting the detection point to implement this is easily accomplished by using a local oscillator and heterodyne detection [6,7]. Figure 9 shows that the required local oscillator can be obtained by using a leaky polarizing beam splitter to pick off the detection beam. Due to the nonunity transmission coefficient of the polarizing beam splitter for $\hat{x}$ polarization, a small fraction of the bright port field leaks into the

detection direction. This leak is in the orthogonal polarization to the (dark port) signal and is perfectly path length matched to the signal.

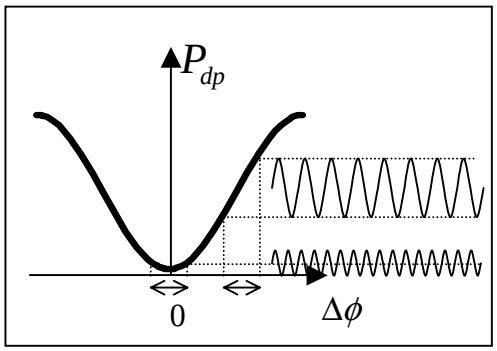

Figure 8: Moving to a linear region of the response function has a considerable advantage in terms of signal size. The signal also appears at the same frequency as the sample modulation.

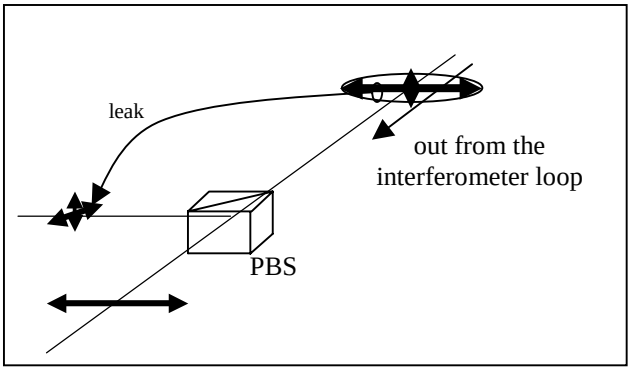

Figure 9: Due to nonunity transmission of horizontal polarization, the polarizing beam splitter leaks a portion of bright port light toward the detection path to the left. This provides the required local oscillator.

To shift detection into the linear regime, either the signal or the local oscillator should be retarded by one quarter wave before the two are mixed with a linear polarizer or a polarizing beam splitter. Defining the power coefficient of the leak of plane polarization from polarizing beam splitter as α, the local oscillator is given by

$$E_{LO} = \sqrt{\alpha} E_{bp} = \sqrt{\alpha} E_0 (\cos \omega t + \cos(\omega t + \Delta\phi))$$

After going through a quarter wave plate,

$$E_{LO} = \sqrt{\alpha} E_0 (\sin \omega t + \sin(\omega t + \Delta\phi))$$

After the signal is mixed with this local oscillator, the detected output is sensitive to noise in the probe laser amplitude E_0. Therefore balanced detection should be employed [8] with an additional half wave plate (rotating 45°) and an additional polarizing beam splitter as shown in Figure 10.

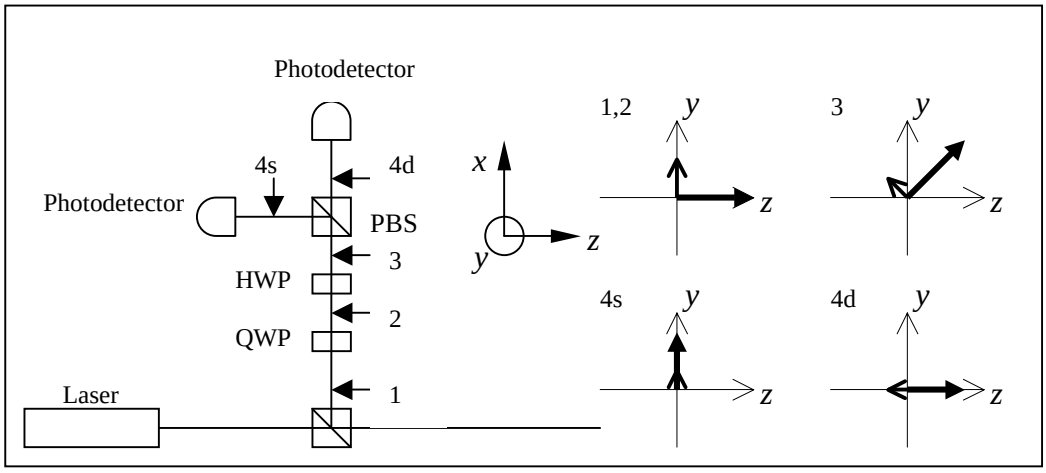

Figure 10: Illustration of the detection port optics when balanced detection with a local oscillator is implemented.

After the signal is combined with the local oscillator at the polarizing beam splitter, the sum port and difference port signals are given by the usual analysis of balanced heterodyne detection as follows:

$$E_{sum} = (E_{LO} + E_{dp})/\sqrt{2}$$

$$P_{sum} \equiv \overline{E_{sum}{}^2} = \frac{1}{2}E_0^2[\alpha + 1 + 2\sqrt{\alpha}\sin\Delta\phi + (\alpha - 1)\cos\Delta\phi]$$

$$E_{diff} = (E_{LO} - E_{dp})/\sqrt{2}$$

$$P_{diff} \equiv \overline{E_{diff}{}^2} = \frac{1}{2}E_0^2[\alpha + 1 - 2\sqrt{\alpha}\sin\Delta\phi + (\alpha - 1)\cos\Delta\phi]$$

After electronic subtraction, the resulting difference photocurrent is given by

$$i_{sig} = e\eta(\frac{\Delta P}{h\nu}) \approx e\eta(\frac{P_{sig}}{h\nu})$$

$$\Delta P = P_{sum} - P_{diff} \cong 2\sqrt{\alpha}E_0^2\sqrt{1-C^2} + 2\sqrt{\alpha}E_0^2 C\delta\phi(t) = P^* + P_{sig}$$

$$P_{sig} = 2\sqrt{\alpha}E_0^2 C\delta\phi(t) = 2\sqrt{P_{LO}}\sqrt{\frac{\eta_t P_{in}}{2}}C\delta\phi(t)$$

$$P^* \equiv 2\sqrt{\alpha}E_0^2\sqrt{1-C^2}$$

where η is the quantum efficiency of the photodiode and P^* is the DC current signal generated due to imperfect contrast ratio. Here only P_{sig} provides time-varying signal photocurrent.

With enough local oscillator power, the shot noise can be made to dominate the thermal noise at the photodetector. The noise photocurrent from the probe laser shot noise is given by

$$i_{noise} = \sqrt{2ei_{DC}B}$$

$$i_{DC} = e\eta(P_{DC}/h\nu)$$

$$P_{DC} = P_{sum} + P_{diff} + P^* = P_{dp} + P_{LO} + P^*$$

where P_{LO} represents the local oscillator power and B represents the detection bandwidth. With these equations the signal-to-noise ratio ($SNR = i_{sig}/i_{noise}$) in the shot-noise limited regime can readily be calculated:

$$SNR = \sqrt{\frac{\eta\eta_t P_{LO}P_{in}C^2}{h\nu(P_{dp} + P_{LO} + P^*)B}}\delta\phi$$

To analyze this SNR function, if C is near unity, then P_{dp} and P^* are negligible compared to P_{LO}. In this case the dependence on P_{LO} cancels out as in any other balanced heterodyne detection scheme. Therefore the signal to noise ratio largely scales as the square root of P_{in}. It is remarkable that the optical power the photodiode has to tolerate is only P_{LO}, not the full power P_{in}, yet the SNR scales as the square root of the number of photons in the power P_{in}. This is possible because the dark port is being used for detection, and a similar advantage will be critical to the successful operation of a gravitational wave interferometer detector.

To obtain the minimum detectable signal, we use the criterion of SNR=1. The resulting shot-noise limited minimum detectable phase shift normalized by the square root of detection bandwidth can be obtained as

$$\frac{\delta\phi}{\sqrt{B}} = \sqrt{\frac{h\nu(P_{dp} + P_{LO} + P^*)}{\eta\eta_t P_{LO}P_{in}C^2}}$$

As can be seen from this expression, one way to increase sensitivity other than having C near unity is to increase the probe laser power P_{in}. In addition, reducing the focal spot size at the sample also generates more phase shift per molecule as explained in Section 2. In optimizing the probe laser power and spot size in order to maximize the sensitivity, the saturation intensity of the sample becomes the key limitation. Another way to reduce the minimum detectable phase shift is to minimize the bandwidth B. Fortunately, as a result of the internal modulation scheme we have adopted, the signal can be averaged as long as necessary in principle. In practice, the requirement for dynamical information and the patience of the experimenter will set a limit on the integration time.

6. EXPERIMENTAL RESULTS

In order to test the feasibility of these ideas, a polarization Sagnac interferometer was constructed with a Pockels cell driven by a sinusoidal RF voltage in the loop as a test sample. The schematic of the setup is illustrated in Figure 11. A spatial filter (SF) was placed before the interferometer loop in order to enhance the contrast ratio (C), as all of the concepts presented earlier about common mode rejection only apply to a single transverse mode of the optical field. The contrast ratio was measured to be 0.9, limited by the spatial filter alignment and static birefringence in the Pockels cell. A 13 mW HeNe laser was used as a probe, and after the optical isolator the power was 10 mW. The transmission factor η_t was measured to be 0.35. The PBS at the detection port leaks about 3% of the major axis polarization, which provides 0.1 mW local oscillator power. In this proof-of-principle demonstration, the balanced detection was not implemented, no molecular sample was present, and the pulsed laser was not used, so only the best-case noise performance can be characterized. The local oscillator and the signal were mixed with a linear polarizer (LP) and only one Si photodiode detector with transimpedance amplifier was used to detect the dark port signal.

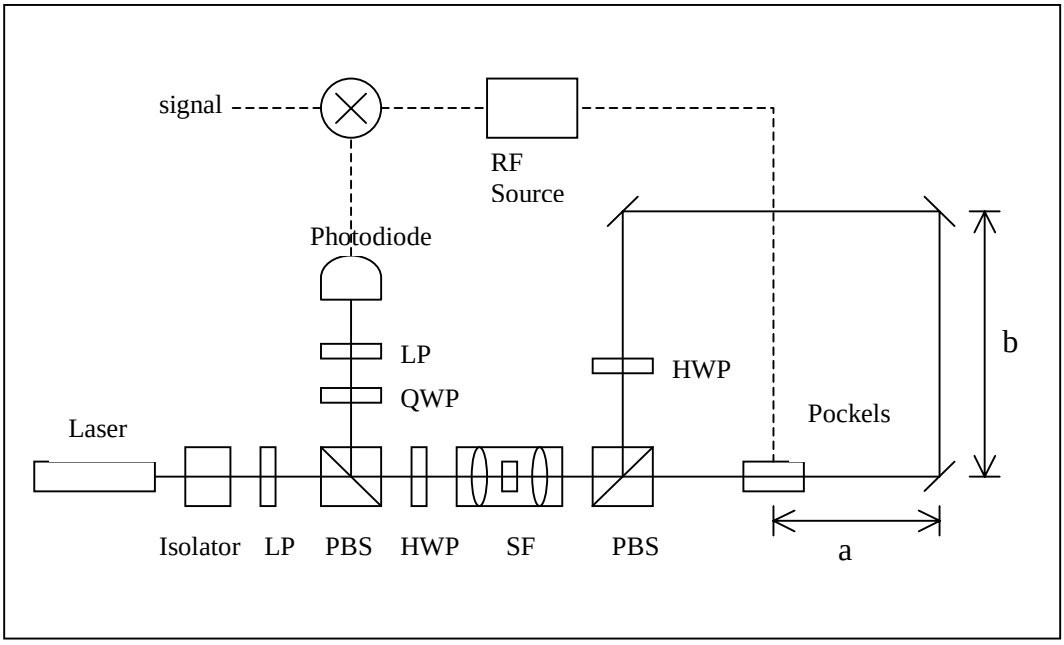

Figure 11: Experimental setup of proof of principle measurement. Note the Pockels cell takes the place of the sample and the pulsed laser of our proposed scheme.

In the case that the Pockels cell is driven with RF frequency ω, the output of the interferometer in terms of the signal current at the modulation frequency ω is proportional to $\left|\sin\left(\omega L/2c\right)\right|$. Here L is the effective loop length, $L = 2(a+b)$. L was set at 183 cm in order to maximize the response at 82 MHz (the mode-locked laser repetition frequency). Figure 12 shows the frequency response of the detected signal from the interferometer as the RF frequency driving the Pockels cell is swept. One can see that the

envelope of the response follows the expected shape. The superimposed modulation is due to the RF path difference between the path from the RF source to the Pockels cell and the path to the demodulation circuit.

With $\eta_t = 0.35$, $\eta = 0.7$, $P_{in} = 10$ mW, $C = 1$ and $P_{dp} = P^* = 0$, the minimum detectable phase shift in the shot noise limit would be expected to be $\delta\phi/\sqrt{B} = 1.13\times10^{-8} rad/\sqrt{Hz}$. Figure 13 shows the measured noise floor for various detection bandwidths. For calibration, a phase shift value of 5 x 10^{-8} rad would correspond to 10 Cy5 molecules. The measured noise floor is $5\times10^{-8} rad/\sqrt{Hz}$. Non-ideal behavior placed the noise floor 5 times above shot noise limit, partly due to the use of unbalanced detection. One fact to note is that the expected inverse square root dependence on the bandwidth is maintained below 1 Hz, as expected from the use of internal modulation. This is an improvement over conventional FM spectroscopy where the bandwidth scaling is only valid above several kHz due to RAM (residual amplitude modulation) from the electro-optic modulator.

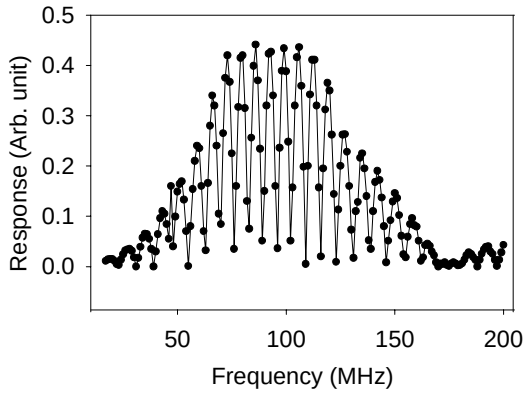

Figure 12: Frequency response of the polarization Sagnac interferometer. The high frequency modulation illustrates the RF phase sensitivity of the detection circuit.

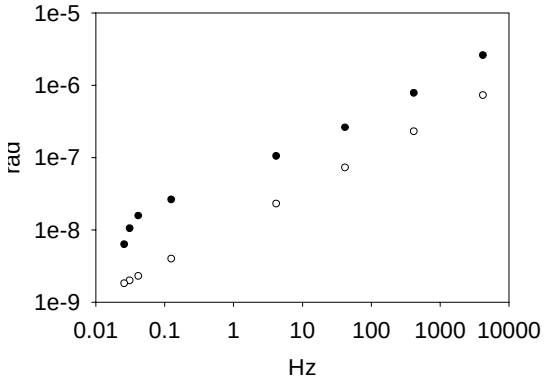

Figure 13: Measured noise floor (closed circles) for corresponding detection bandwidths. With 3.5mW effective probe power and without balanced detection, the noise floor is 5 times above the minimum value expected in the shot noise limit (open circles).

7. SUMMARY AND CONCLUSION

We have presented a proposal for the detection of ultrasmall phase shifts in a condensed phase sample using Sagnac interferometry coupled with time-dependent optical saturation of the spectral feature with a pump laser. Specific optical measurements have yielded a detection limit of $5\times10^{-8} rad/\sqrt{Hz}$, which is expected to improve in several ways. First, higher optical power will yield a lower detection limit scaling as the inverse square root of the probe power. Second, improved optical components that maintain the single-mode character in the loop will increase the contrast ratio. Finally, balanced detection will render the system less sensitive to technical laser noise, thus allowing the shot-noise limit to be approached much more closely.

It is worthwhile to note several appealing aspects of this proposed method. First, the wavelength at which saturation must be performed can be considerably away from the wavelength of maximum phase shift, so that the pumping and probing beams can be easily separated. Second, the power of the probe beam can be increased considerably without causing saturation of the absorption compared to the case where direct absorption is measured. Third, this method lends itself easily to scanning of the sample to build up an image of the absorption. Finally, the polarization Sagnac has the distinct advantage of being able to obtain a low detection limit without an extremely high power on the detector. Experiments are in progress to demonstrate all the ideas presented in this paper with a molecular dopant in a solid matrix, with the goal of reaching a detection limit of 100 molecules or less in 1 Hz bandwidth a likely possibility.

8. ACKNOWLEDGEMENT

The authors warmly thank M. D. Fayer for providing a mode-locker, M. Digonnet for the loan of a Nd-YAG laser, and J. Schleier-Smith and S. Goda for consultation and optical assistance. This work was supported in part by the Defense Advanced Research Projects Agency Grant No. MDA972-00-1-0032 and by the National Science Foundation Grant No. 0241012.

9. REFERENCES

1. W. E. Moerner and L. Kador, "Optical Detection and Spectroscopy of Single Molecules in Solids," *Phys. Rev. Lett.* **1989**, *62*, 2535.
2. Sun, K-X.; Fejer, M. M.; Gustafson, E.; Byer, R. L. “Sagnac Interferometer for Gravitational-Wave Detection,” *Phys. Rev. Lett.* **1996**, *76*, 3053-3056.
3. Beyersdorf, P. T.; Fejer, M. M.; Byer, R. L. “Polarization Sagnac Interferometer with Postmodulation for Gravitational-Wave Detection,” *Opt. Lett.* **1999**, *24*, 1112-1114.
4. Yariv, A., Optical Electronics in Modern Communications, (New York, Oxford University Press, 1997), pp. 171-175.
5. G. Sagnac, C. R. Acad. Sci. **1913**, *95*, 1410.
6. Beyersdorf, P. “The Polarization Sagnac Interferometer for Gravitational Wave Detection,” Ph.D. Dissertation, Stanford University, (January 2001).
7. Beyersdorf, P. T.; Fejer, M. M.; Byer, R. L. “Polarization Sagnac Interferometer with a Common-Path Local Oscillator for Heterodyne Detection,” *J. Opt. Soc. Am. B* **1999**, *16*, 1354-1358.
8. Sun, K-X.; Fejer, M. M.; Gustafson, E.; Byer, R. L. “Balanced Heterodyne Signal Extraction in a Postmodulated Sagnac Interferometer at Low Frequency,” *Opt. Lett.* **1997**, *22*, 1485-1487.